Supplementary Information

Assembly of sandwiched-type ruthenium-containing polyoxometalates for efficient construction of C-C bonds

Lijuan Xiong, Sen Liu, Wenjing Chen, Mengnan Yang, Pengtao Ma, Jingping Wang,* and Jingyang Niu*

Henan Key Laboratory of Polyoxometalate Chemistry, College of Chemistry and Chemical Engineering, Henan University, Kaifeng, Henan 475004, China

I. Experimental Section

II. Supplementary Structure Figures and Characterizations

Fig. S1 Schematic synthetic process of **Ru_4W_{18}**.

Fig. S2 Comparison of connection modes in sandwiched-type polyoxotungstate clusters.

Fig. S3 Planar diagram and the bond length of Ru-Ru.

Fig. S4 The molecular structure of **Ru_4W_{18}**.

Fig. S5 Photograph of compound **Ru_4W_{18}**.

Fig. S6 FT-IR spectrum and PXRD patterns of **Ru_4W_{18}** and paratungstate

Fig. S7 The XPS spectra of **Ru_4W_{18}**.

Fig. S8 TGA spectra of **Ru_4W_{18}**.

Fig. S9 Hot filtration test and Recycling experiments for the Knoevenagel condensation.

Fig. S10 PXRD pattern and FT-IR spectrum collected after the catalytic reactions of catalyst **Ru_4W_{18}** in Knoevenagel condensation.

Fig. S11 FT-IR spectrum of P_2W_{19}.

Fig. S12-S21 ^{1}H NMR spectra of compound 3 and other substrate scope products in the Knoevenagel condensation reaction.

Fig. S22-S34 The GC-MS spectrum of compound 3 and other substrate scope products in the Knoevenagel condensation reaction.

III. Supplementary Tables

Table S1. Crystal data for compound $\mathbf{Ru_4W_{18}}$.

Table S2. BVS values of Ru and W atoms of $\mathbf{Ru_4W_{18}}$.

Table S3. Selected bond distances of compound $\mathbf{Ru_4W_{18}}$.

Table S4. Selected bond angles (°) of compound $\mathbf{Ru_4W_{18}}$.

Table S5. Comparison of the catalytic efficiency of different heterogeneous catalysts.

References

I. Experimental Section

Materials and physical measurements

All chemicals were purchased commercially without further purification. The precursor P_2W_{19} was obtained from published sources, and its identity was confirmed by means of IR spectroscopy.[1] Elemental analyses (H) were recorded by means of an Elementar VarioELcube CHNS analyzer. The single-crystal data were obtained by means of a Bruker D8 VENTURE PHOTON II CCD diffractometer with Mo Kα radiation (the value of λ was 0.71073 Å) in the cooled nitrogen flow at 150 K. The X-ray powder diffraction (PXRD) patterns were obtained using a Bruker D8 ADVANCE diffractometer with a measurement range of 2θ angles from 5 to 50°, employing Cu Kα radiation (wavelength λ = 1.54056 Å). IR spectra were recorded using KBr pellets on a Bruker TENSOR II FT-IR in the range of 4000–500 cm^{-1}. Thermogravimetric analysis (TGA) was performed using a NETZSCH STA 449 F5 Jupiter thermal analyser in a nitrogen atmosphere over the temperature range of 25 to 800 °C at a heating rate of 10 °C min^{-1}. A Perkin Elmer Optima 2100 DV spectrometer was selected for inductively coupled plasma-atomic emission spectrometry (ICP-AES) analyses (K, Na, Ru and W). X-ray Photoelectron Spectroscopy (XPS) was measured on a Thermo Scientific K-Alpha spectrometer with monochromatic aluminium (hν = 1486.6 eV) serving as the excitation source. GC-MS (Agilent 7890B GC/5973B MS, SE-54 capillary column) and GC analyses were determined on a Bruker 450-GC with a flame ionization detector and a 30 m column with nitrogen as the carrier gas. ^{1}H NMR spectra were recorded on a Bruker AVANCE NEO 500 MHz NMR spectrometer.

X-ray Crystallography

Some suitable shapes crystal with appropriate size were selected and placed on a Bruker D8 VENTURE PHOTON II CCD diffractometer. The radiation source of graphite-monochromated Mo Kα (λ = 0.71073 Å) was used to collect the crystal data in the cooled nitrogen flow at 150 K. The SHELXT structure solution program was used to solve all the structures, and the SHELXL refinement package in Olex2 was used for the full-matrix least-squares algorithm on F^2 data.[2, 3] In the final refinement cycle, the Ru, W, O, Na and K atoms were refined into anisotropy. CCDC contains the

supplementary crystallographic data for this paper with deposition number 2504002 for **Ru_4W_{18}**. The crystallographic data can be obtained free of charge from The Cambridge Crystallographic Data Center via http://www.ccdc.cam.ac. uk/data_request/cif.

Material Preparation: $K_8Na_3H_9[Ru_4O_4\{W_9O_{33}\}_2]\cdot 30H_2O$

Solid $K_{14}[P_2W_{19}O_{69}(H_2O)]\cdot 24H_2O$**{$P_2W_{19}$}** (10.02 g, 1.77 mmol), $Na_2WO_4\cdot 2H_2O$ (10.24 g, 0.031 mol), Na_2SeO_3 (0.55 g, 3.2 mmol), KCl (5.00 g, 0.067 mol) and $RuCl_3\cdot 3H_2O$ (4.00 g, 0.0153 mol) were successively dissolved in 175 mL of 1M malonic acid solution. The mixed solution was vigorously stirred at room temperature for 30 minutes and then packed into the reaction container in 10ml each, and the pH of the solution was adjusted to 2.47-2.53 with 6 M NaOH. Next, 4-methylnicotinic acid (58 mg, 0.423 mmol) and 1mL 1 M LiOH were added to the resulting solution and stirred at room temperature for 1 hour. The solution was subsequently transferred into a 25 mL Teflon-lined autoclave and heated at 160 °C for 72 hours. After cooling to room temperature, the solution was filtered and evaporated slowly. The black rod-shaped crystals were obtained after one week. Yield: 0.66% (7 mg, based on Ru). Elemental analysis calcd. (%) for **Ru_4W_{18}**: K 5.43；Na1.20；Ru 7.01；W 57.40；H 1.21. Found: K 5.41；Na 1.18；Ru 7.02；W 57.45；H 1.23. IR (KBr pellet, cm^{-1}): 3518, 3435, 3366, 1626, 938, 883, 836, 699, 616, 520.

General procedure for the catalysis

Knoevenagel condensation: In a test tube at a temperature of 70°C, the following reagents should be added: aldehyde (1.5 mmol), ethyl cyanoacetate (1 mmol), ethanol (1 mL), and catalyst **Ru_4W_{18}** (1 μmol). The reaction mixture was subjected to stirring and heating under specified conditions in a parallel reactor. The product was identified by gas chromatography-mass spectrometry (GC-MS) and the yields were measured by GC using methylbenzene as an internal standard. The catalyst was then subjected to a thorough washing procedure, consisting of three rinses with ethanol. Subsequent to this, it was dried under vacuum conditions at a temperature of 60°C.

II. Supplementary Structure Figures and Characterizations

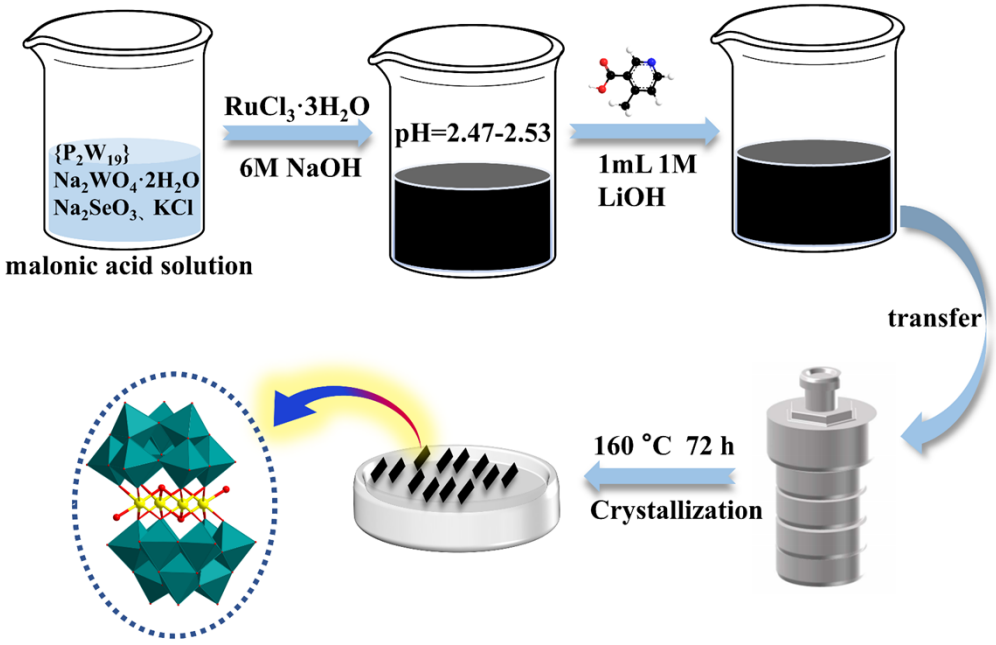

Fig. S1 Schematic synthetic process of compound $\mathbf{Ru_4W_{18}}$.

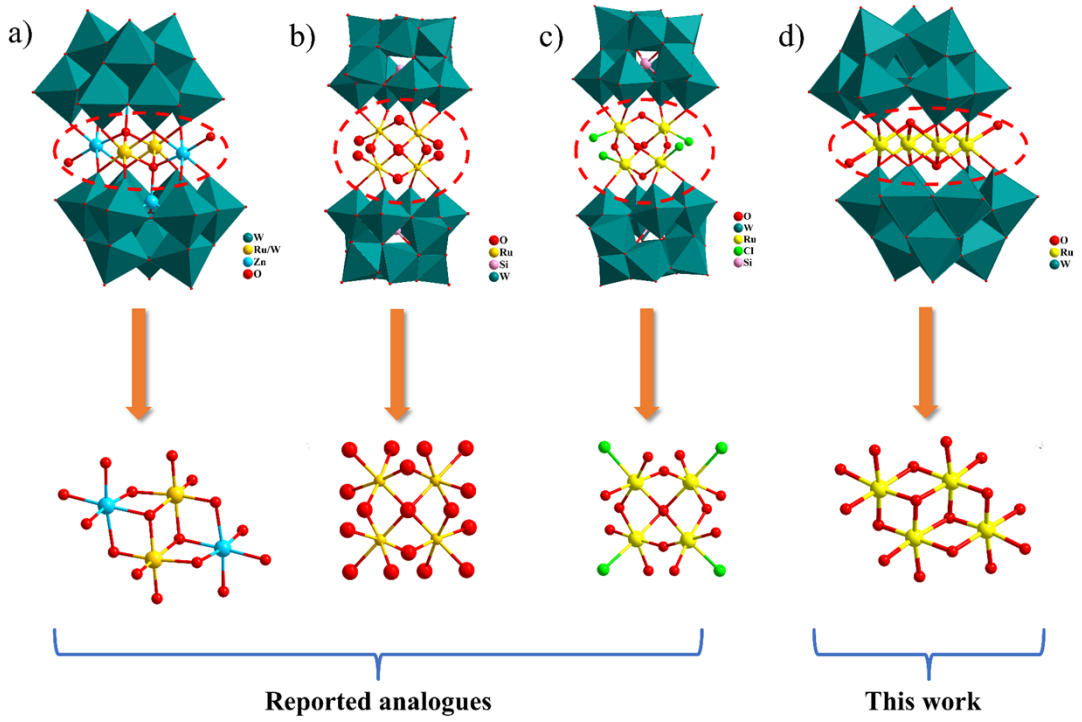

Fig. S2 Comparison of four different connection modes in sandwich tungsten clusters: (a) $[Ru^{III}_2Zn_2(H_2O)_2(ZnW_9O_{34})_2]^{14-}$;[4] (b) $[\{Ru^{IV}_4O_4(OH)_2(H_2O)_4\}(\gamma\text{-}SiW_{10}O_{36})_2]^{10-}$ and $[(\gamma\text{-}PW_{10}O_{36})_2\{Ru^{IV}_4O_5(OH)(H_2O)_4\}]^{9-}$;[5-7] (c) $[Ru^{IV}_4Cl_4O_2(\mu\text{–}OH)_4(\gamma\text{-}SiW_{10}O_{36})_2]^{12-}$;[8] (d) $[Ru_4O_4\{W_9O_{33}\}_2]^{20-}$ (this work).

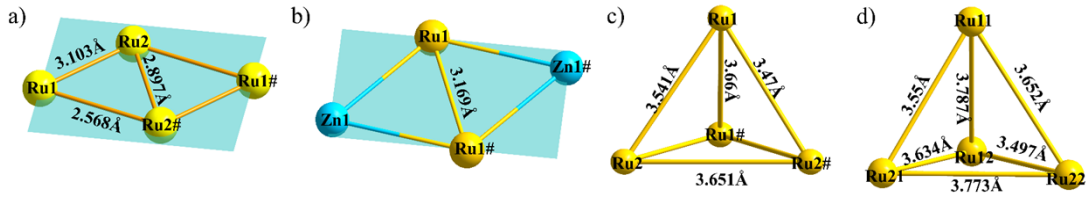

Fig. S3 (a) Planar diagram of $\{Ru_4\}$ and the bond length of Ru-Ru; (b) Planar diagram of $\{Ru_2Zn_2\}$ and the bond length of Ru-Ru; (c) the bond length of Ru-Ru in $\{Ru^{IV}{}_4O_4(OH)_2(H_2O)_4\}$; (d) the bond length of Ru-Ru in $\{Ru^{IV}{}_4Cl_4O_2(\mu{-}OH)_4\}$.

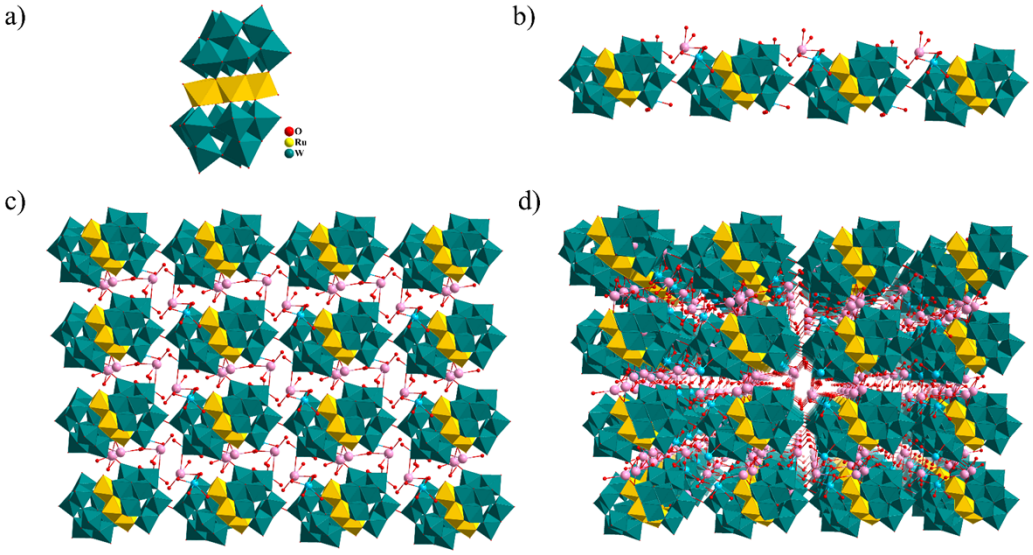

Fig. S4 (a) The molecular structure of $\mathbf{Ru_4W_{18}}$ in polyhedral. (b) Polyhedral and ball-stick representations showing the 1D chain structure; (c) The 2D layer structure of $\mathbf{Ru_4W_{18}}$; (e) 3D supramolecular network of $\mathbf{Ru_4W_{18}}$. Color codes: W, teal; Ru, yellow; O, red; Na, sky blue; K, rose. Polyhedron color: W, teal; Ru: yellow.

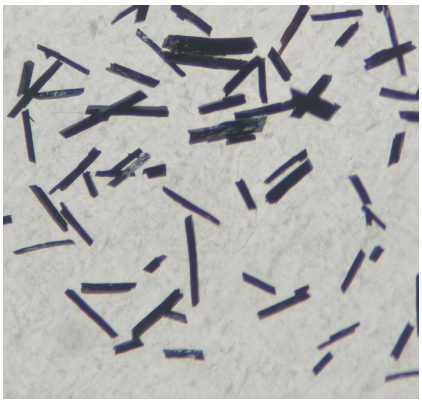

Fig. S5 Photograph of compound $\mathbf{Ru_4W_{18}}$

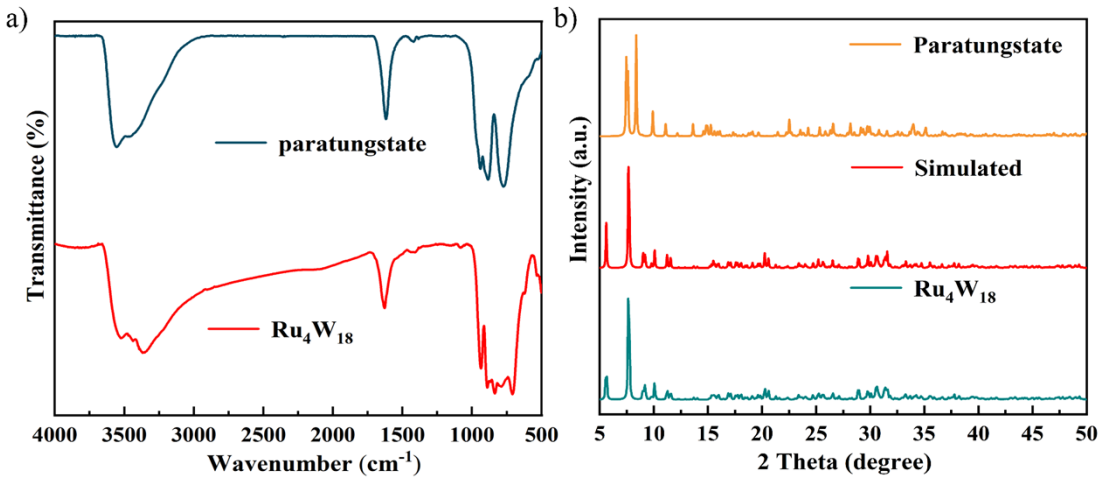

Fig. S6 (a) IR spectrum of $\mathbf{Ru_4W_{18}}$ and paratungstate; (b) PXRD patterns: simulated paratungstate, and experimental and simulated $\mathbf{Ru_4W_{18}}$.

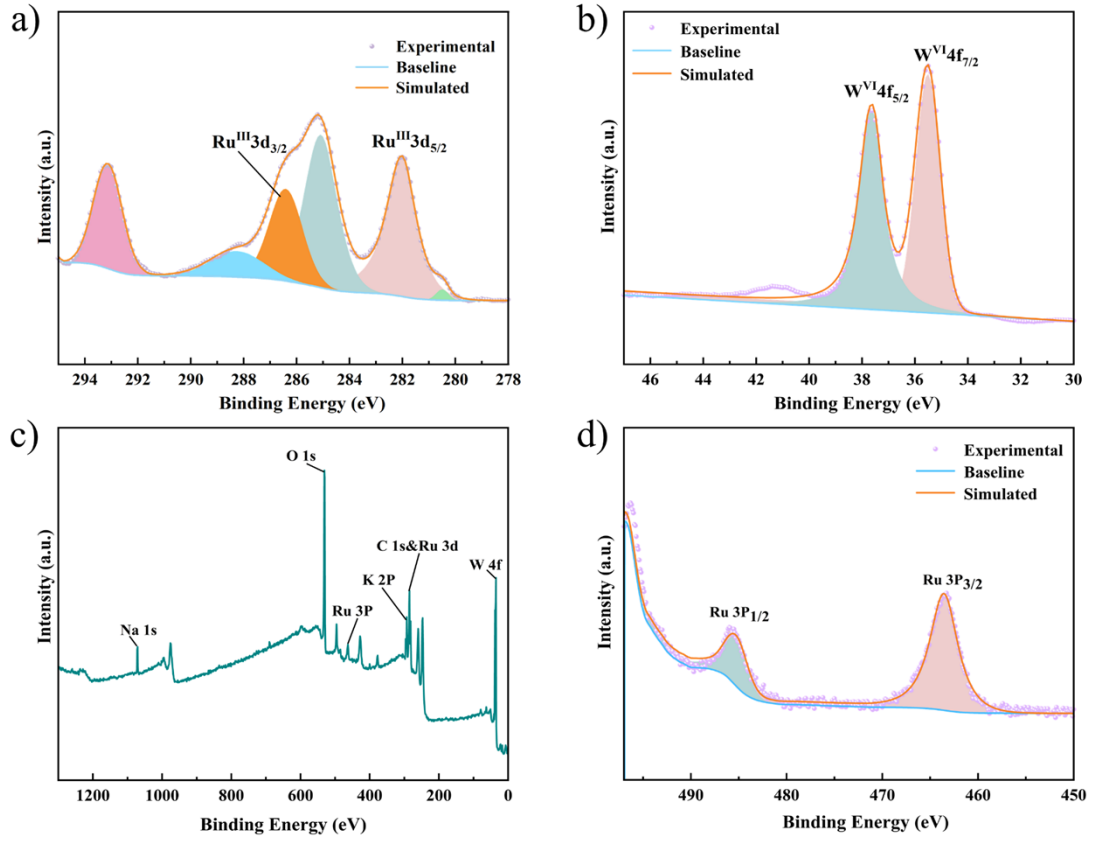

Fig. S7 (a) The XPS spectra of Ru 3d for $\mathbf{Ru_4W_{18}}$; (b) The XPS spectra of W 4f for $\mathbf{Ru_4W_{18}}$; (c) The XPS survey spectra of compound $\mathbf{Ru_4W_{18}}$; (d) The XPS spectra of Ru 3p for $\mathbf{Ru_4W_{18}}$

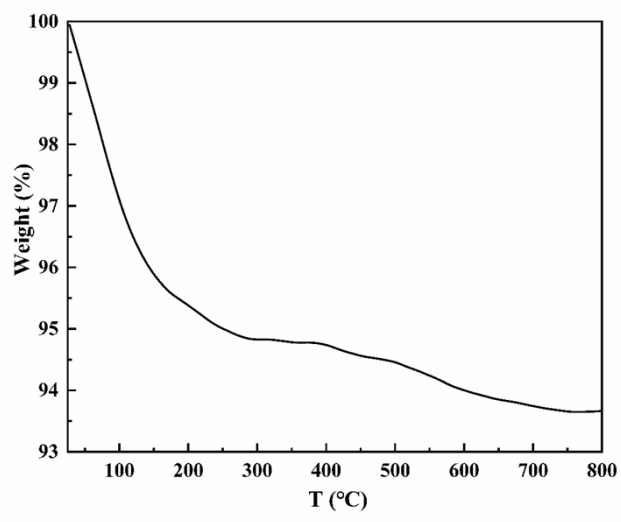

Fig. S8 TGA spectra of $\mathbf{Ru_4W_{18}}$

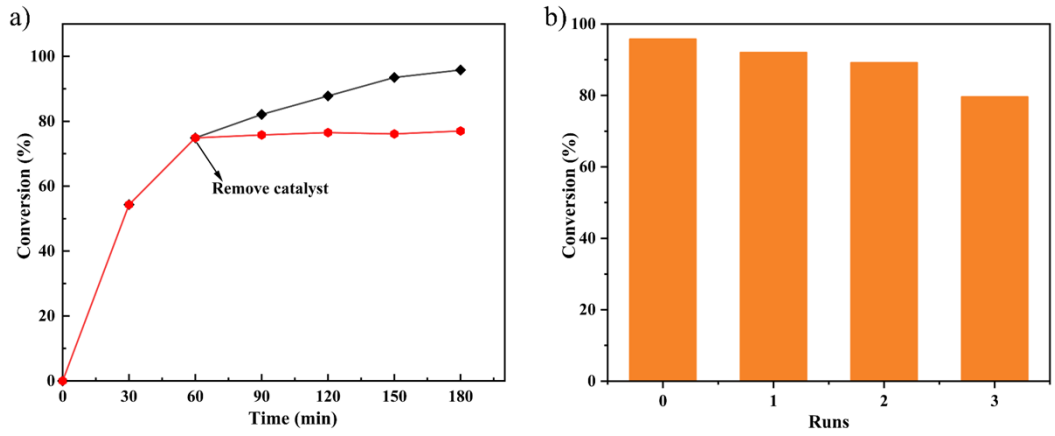

Fig. S9 (a) Hot filtration test; (b) Recycling experiments for the Knoevenagel condensation

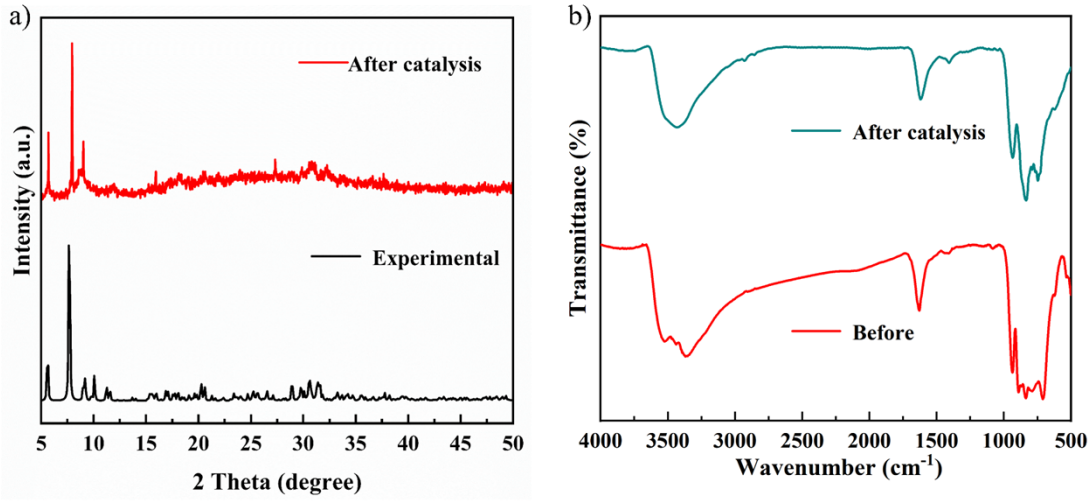

Fig. S10 (a) PXRD pattern and (b) FT-IR spectrum collected after the catalytic reactions of catalyst $\mathbf{Ru_4W_{18}}$ in Knoevenagel condensation

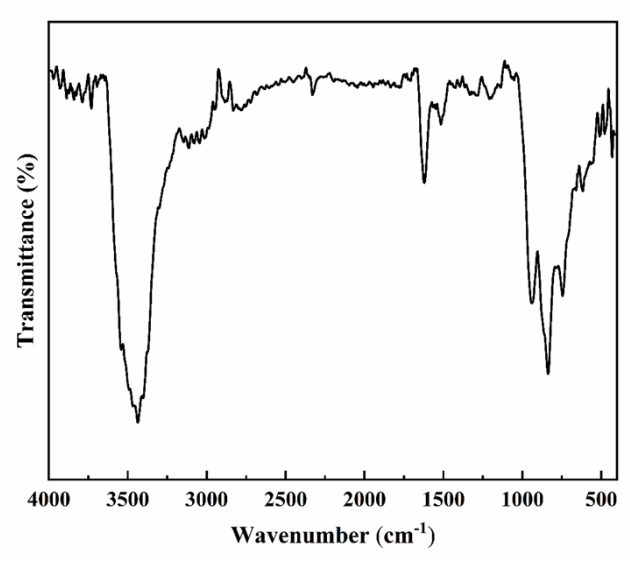

Fig. S11 FT-IR spectrum of P_2W_{19}

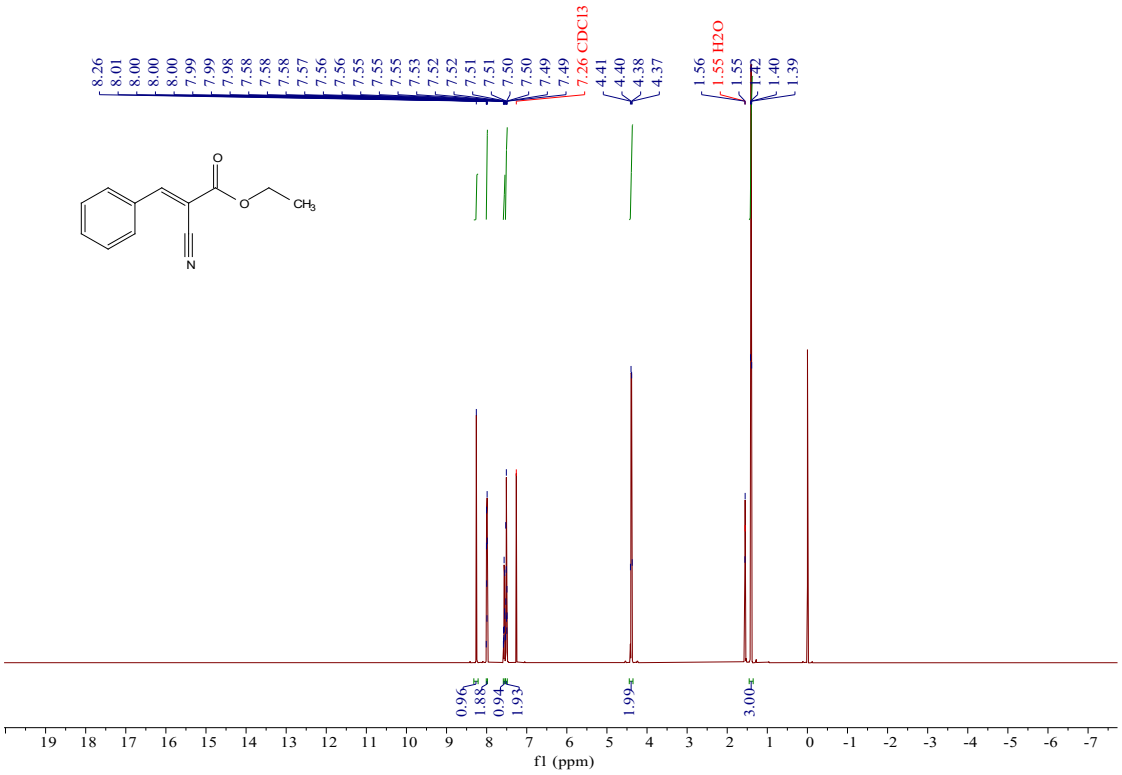

Fig. S12 ^{1}H NMR (500 MHz, CDCl3) δ 8.26 (s, 1H), 8.01 – 7.98 (m, 2H), 7.58 – 7.54 (m, 1H), 7.53 – 7.49 (m, 2H), 4.39 (q, J = 7.1 Hz, 2H), 1.40 (t, J = 7.1 Hz, 3H).

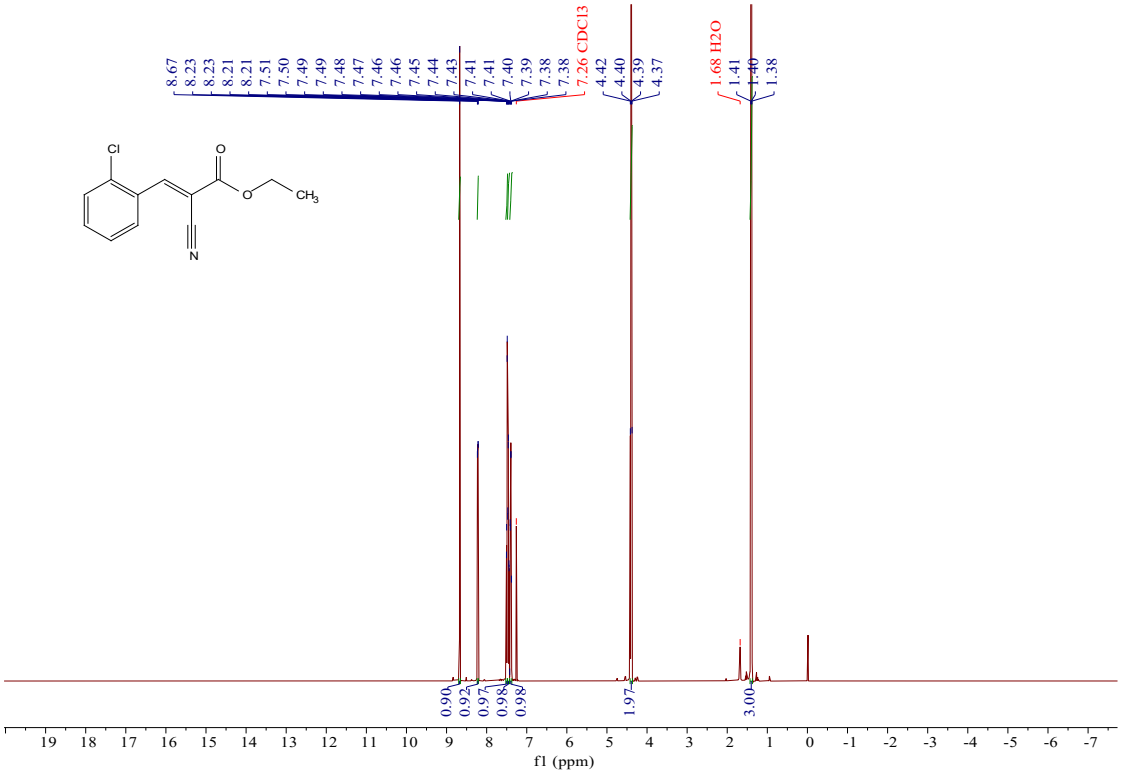

Fig. S13 ^{1}H NMR (500 MHz, $CDCl_3$) δ 8.67 (s, 1H), 8.22 (dd, *J* = 7.9, 1.6 Hz, 1H), 7.50 (dd, *J* = 8.0, 1.5 Hz, 1H), 7.46 (td, *J* = 7.6, 1.7 Hz, 1H), 7.40 (td, *J* = 7.5, 1.5 Hz, 1H), 4.39 (q, *J* = 7.2 Hz, 2H), 1.40 (t, *J* = 7.1 Hz, 3H).

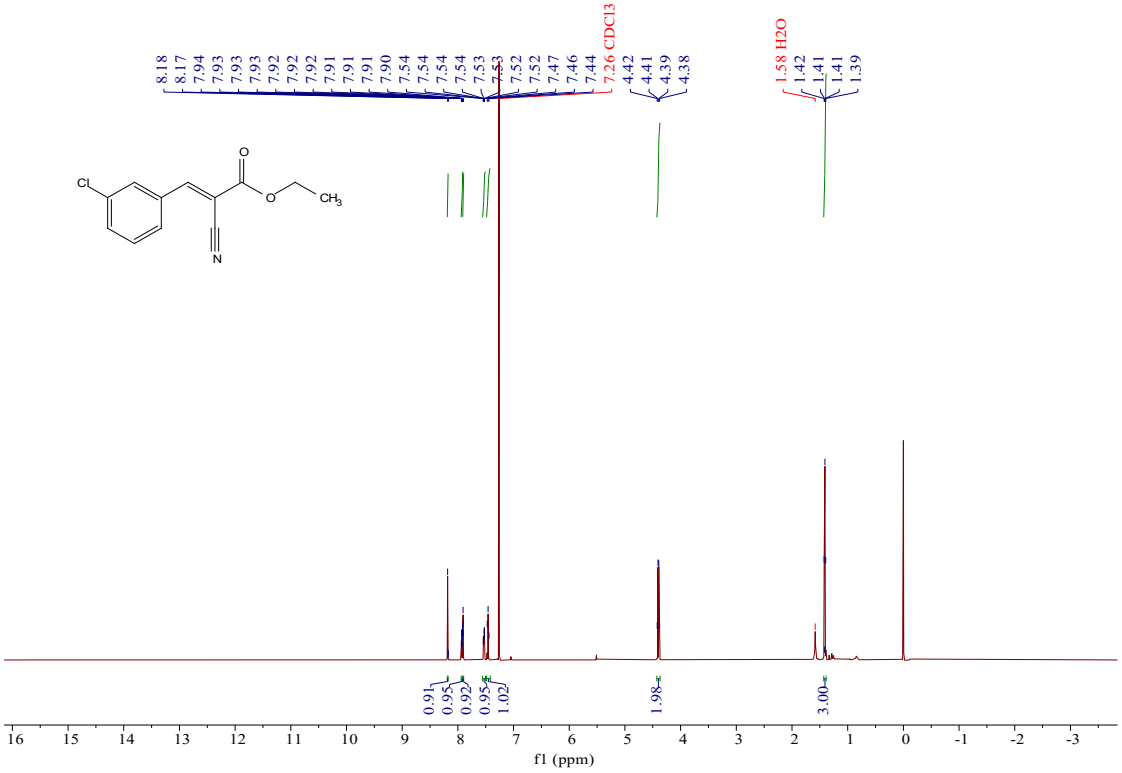

Fig. S14 [1]H NMR (500 MHz, CDCl3) δ 8.18 (s, 1H), 7.93 (dq, J = 7.7, 1.1 Hz, 1H), 7.91 (t, J = 1.9 Hz, 1H), 7.53 (ddd, J = 8.0, 2.1, 1.0 Hz, 1H), 7.46 (t, J = 7.9 Hz, 1H), 4.40 (q, J = 7.1 Hz, 2H), 1.41 (t, J = 7.1 Hz, 3H).

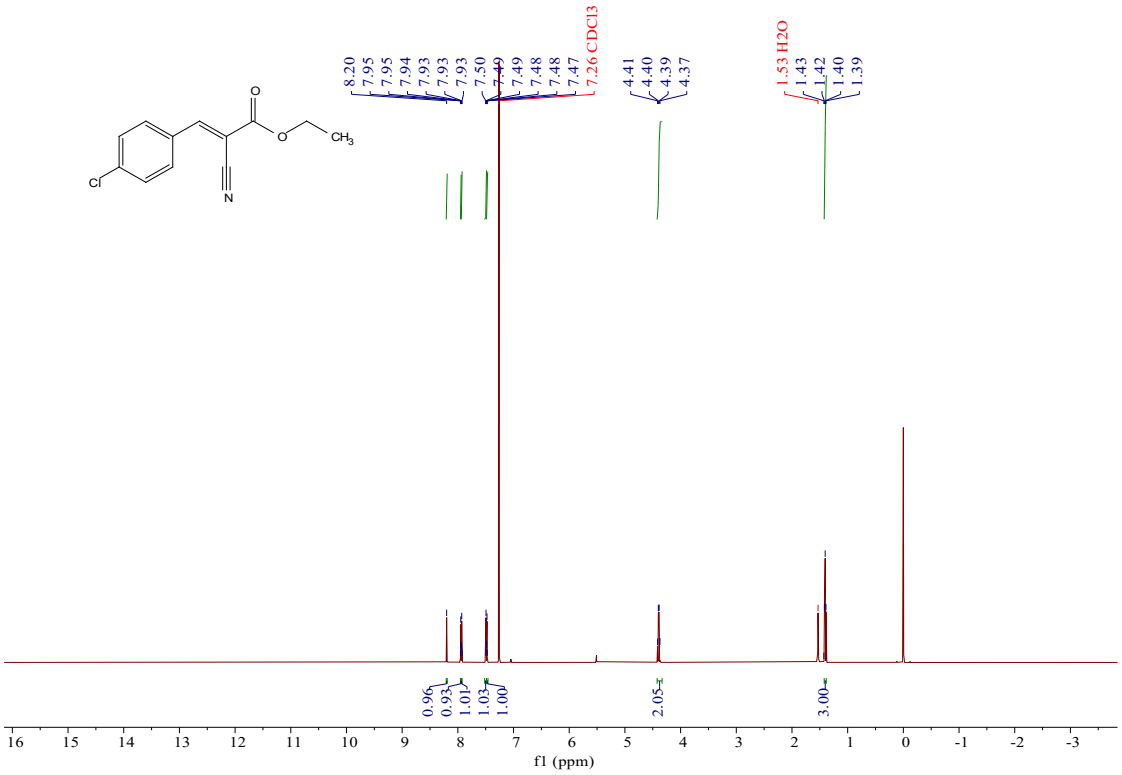

Fig. S15 [1]H NMR (500 MHz, $CDCl_3$) δ 8.20 (s, 1H), 7.95 (d, *J* = 1.9 Hz, 1H), 7.93 (d, *J* = 2.1 Hz, 1H), 7.49 (d, *J* = 2.0 Hz, 1H), 7.48 (d, *J* = 2.0 Hz, 1H), 4.39 (q, *J* = 7.1 Hz, 2H), 1.40 (t, *J* = 7.1 Hz, 3H).

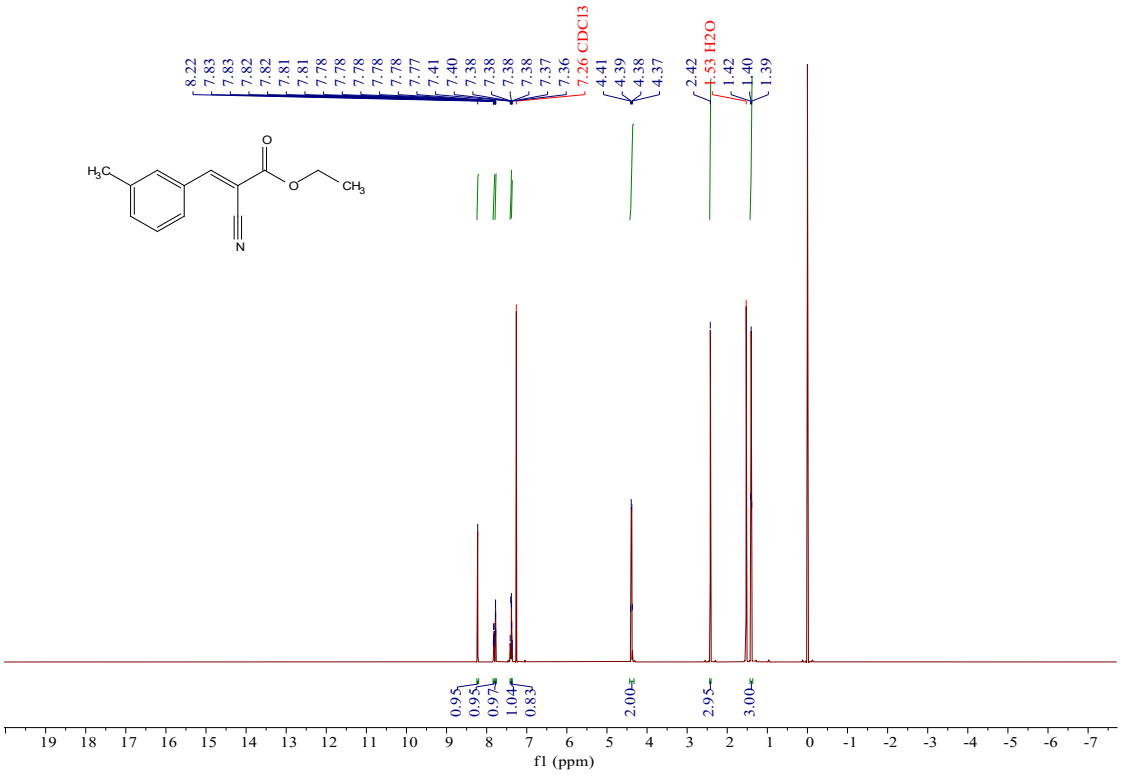

Fig. S16 ^{1}H NMR (500 MHz, $CDCl_3$) δ 8.22 (s, 1H), 7.82 (dt, J = 7.4, 1.9 Hz, 1H), 7.78 (td, J = 1.8, 1.0 Hz, 1H), 7.42 – 7.38 (m, 1H), 7.38 – 7.36 (m, 1H), 4.39 (q, J = 7.1 Hz, 2H), 2.42 (s, 3H), 1.40 (t, J = 7.1 Hz, 3H).

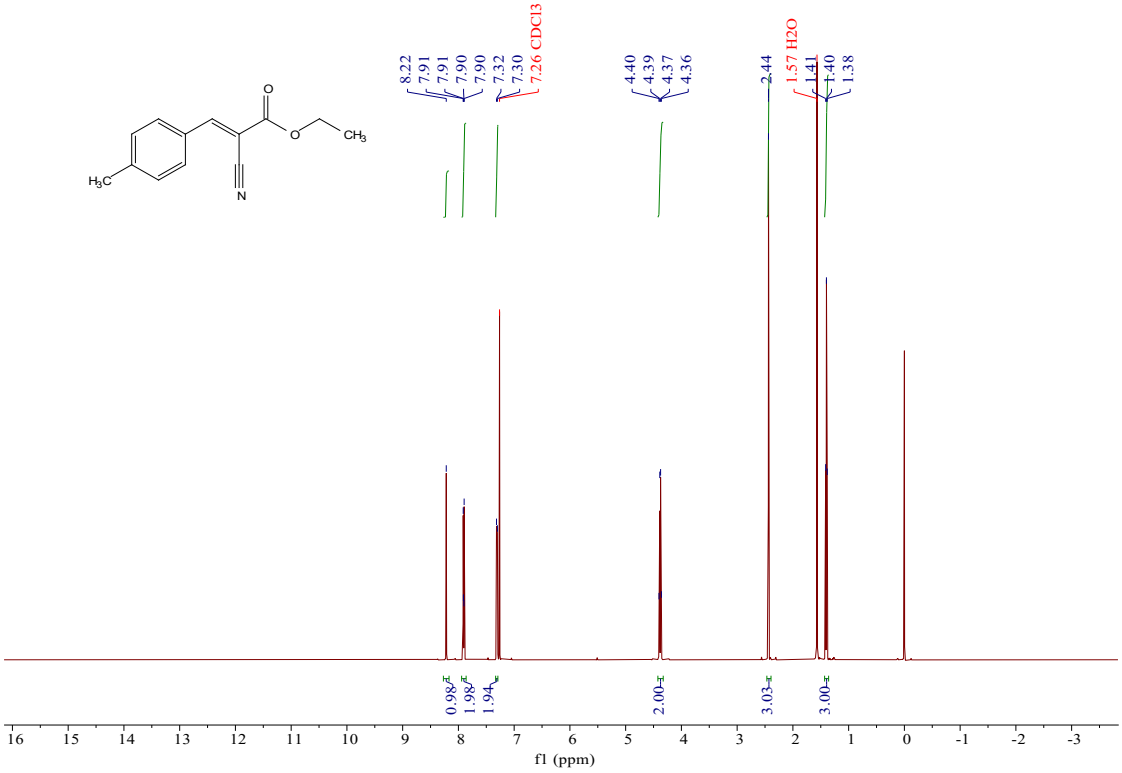

Fig. S17 ^{1}H NMR (500 MHz, $CDCl_3$) δ 8.22 (s, 1H), 7.94 – 7.86 (m, 2H), 7.31 (d, *J* = 8.0 Hz, 2H), 4.38 (q, *J* = 7.1 Hz, 2H), 2.44 (s, 3H), 1.40 (t, *J* = 7.1 Hz, 3H).

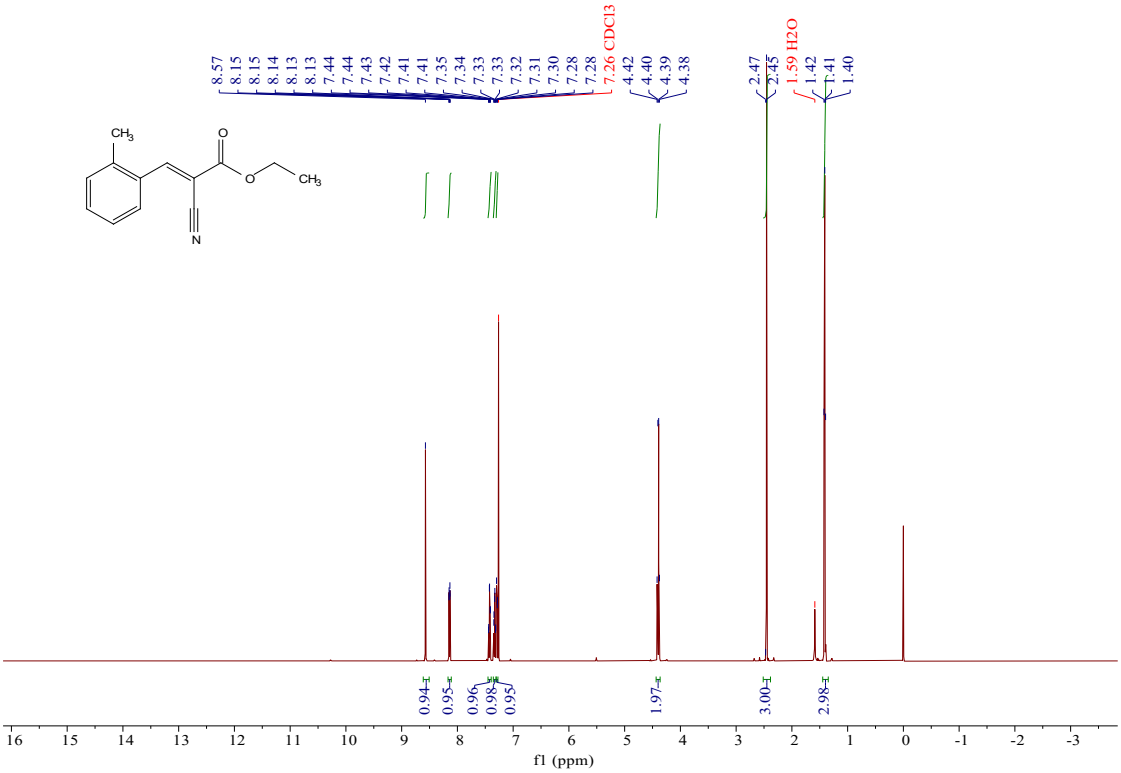

Fig. S18 ^{1}H NMR (500 MHz, $CDCl_3$) δ 8.57 (s, 1H), 8.17 – 8.11 (m, 1H), 7.42 (td, *J* = 7.5, 1.3 Hz, 1H), 7.33 (td, *J* = 7.7, 1.3 Hz, 1H), 7.30 – 7.27 (m, 1H), 4.40 (q, *J* = 7.1 Hz, 2H), 2.45 (s, 3H), 1.41 (t, *J* = 7.2 Hz, 3H).

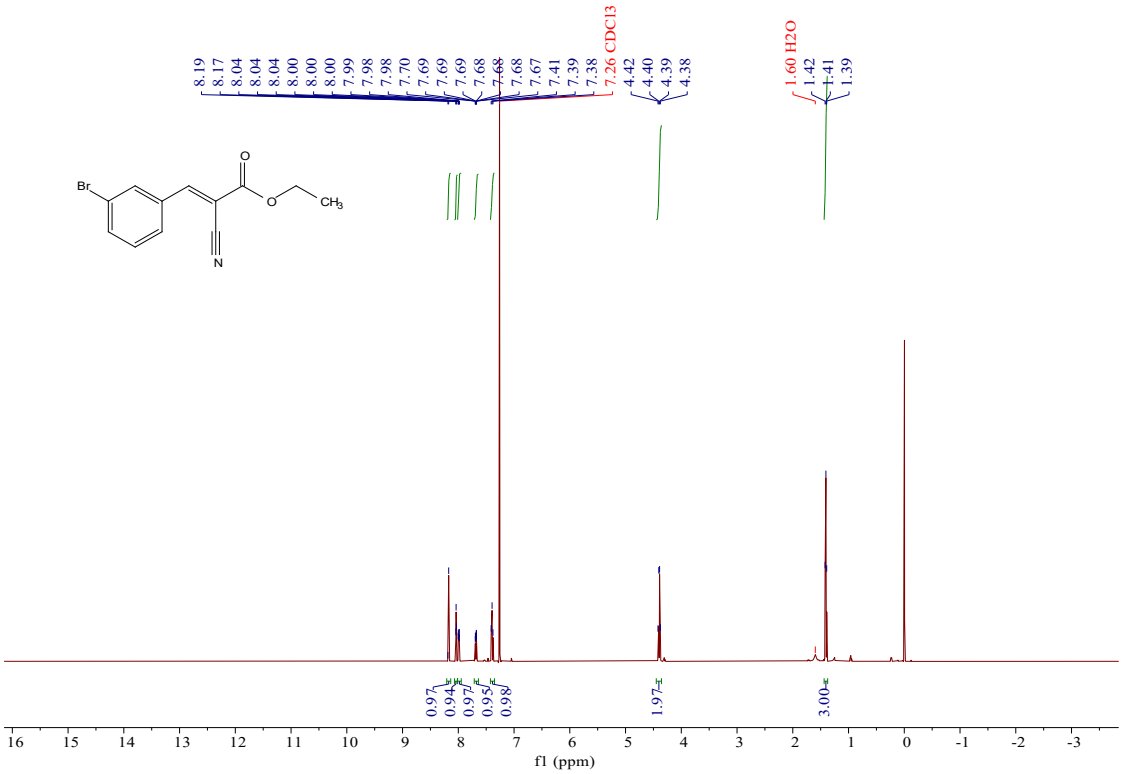

Fig. S19 ^{1}H NMR (500 MHz, $CDCl_3$) δ 8.17 (s, 1H), 8.04 (t, *J* = 1.9 Hz, 1H), 8.01 – 7.95 (m, 1H), 7.68 (ddd, *J* = 8.0, 1.9, 0.9 Hz, 1H), 7.39 (t, *J* = 7.9 Hz, 1H), 4.40 (q, *J* = 7.1 Hz, 2H), 1.41 (t, *J* = 7.1 Hz, 3H).

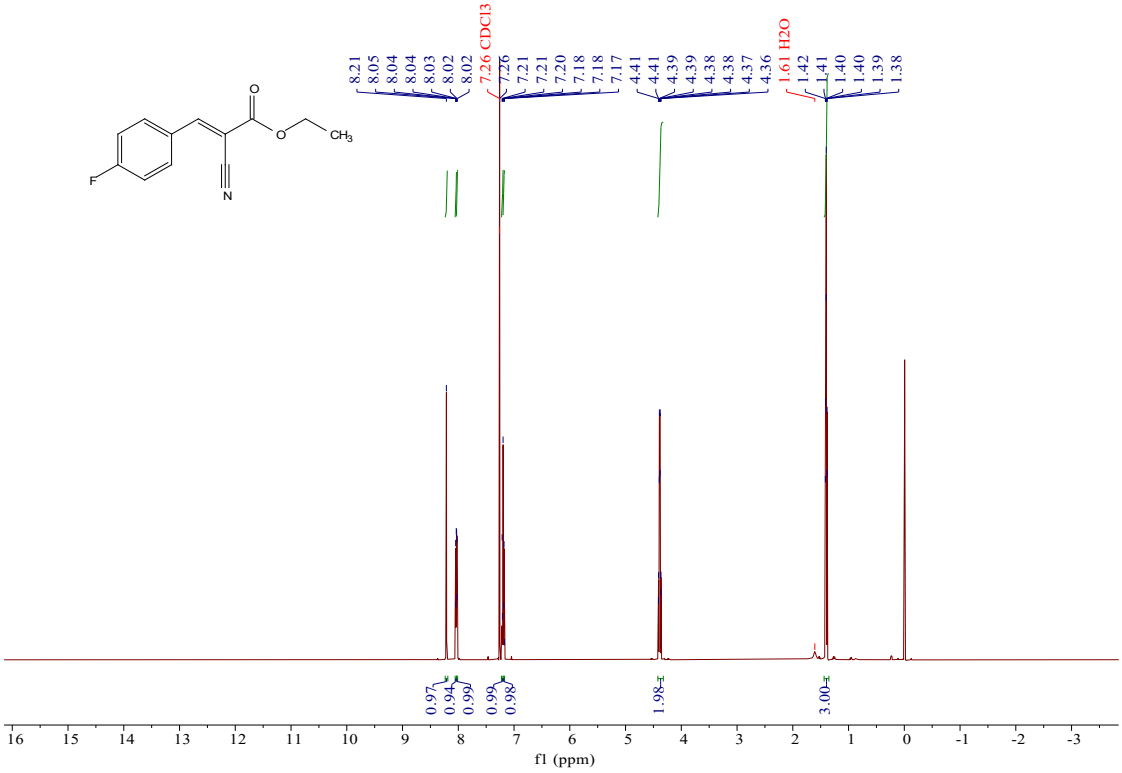

Fig. S20 ^{1}H NMR (500 MHz, $CDCl_3$) δ 8.21 (s, 1H), 8.04 (d, J = 5.4 Hz, 1H), 8.03 – 8.01 (m, 1H), 7.21 (d, J = 8.5 Hz, 1H), 7.18 (d, J = 1.7 Hz, 1H), 4.39 (qd, J = 7.2, 0.9 Hz, 2H), 1.40 (td, J = 7.2, 0.9 Hz, 3H).

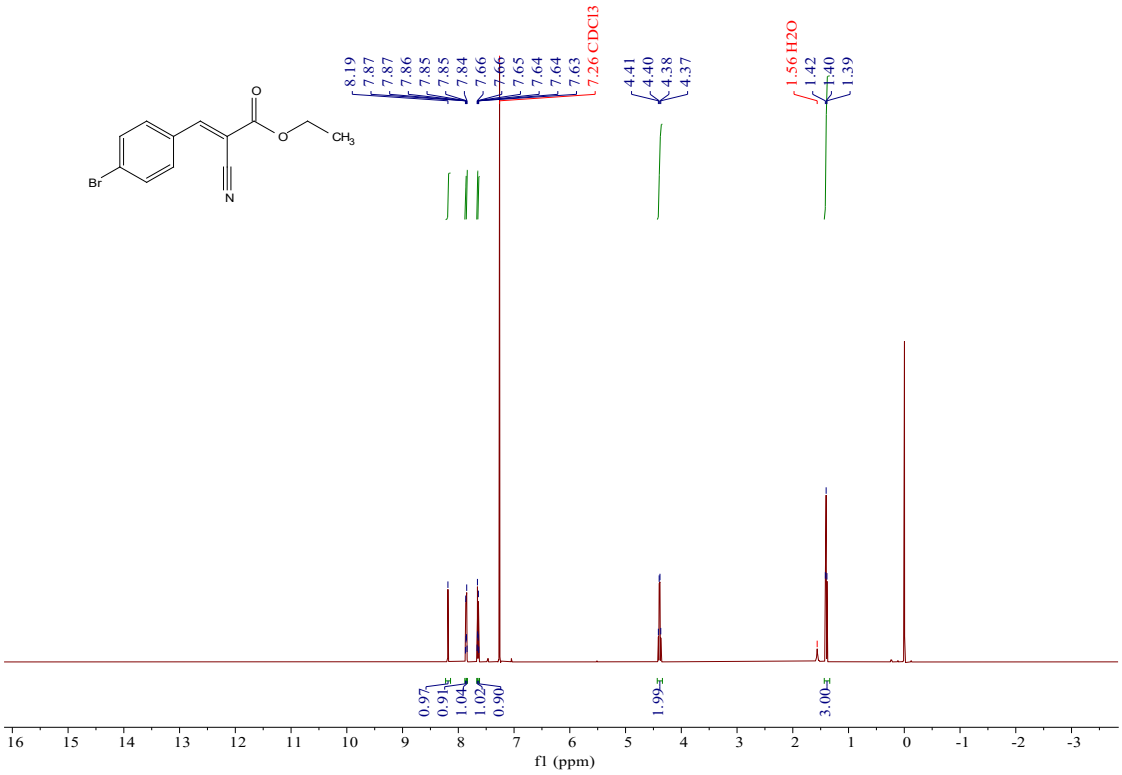

Fig. S21 ^{1}H NMR (500 MHz, $CDCl_3$) δ 8.19 (s, 1H), 7.86 (d, J = 2.1 Hz, 1H), 7.85 (d, J = 2.1 Hz, 1H), 7.65 (d, J = 2.0 Hz, 1H), 7.64 (d, J = 2.0 Hz, 1H), 4.39 (q, J = 7.1 Hz, 2H), 1.40 (t, J = 7.1 Hz, 3H).

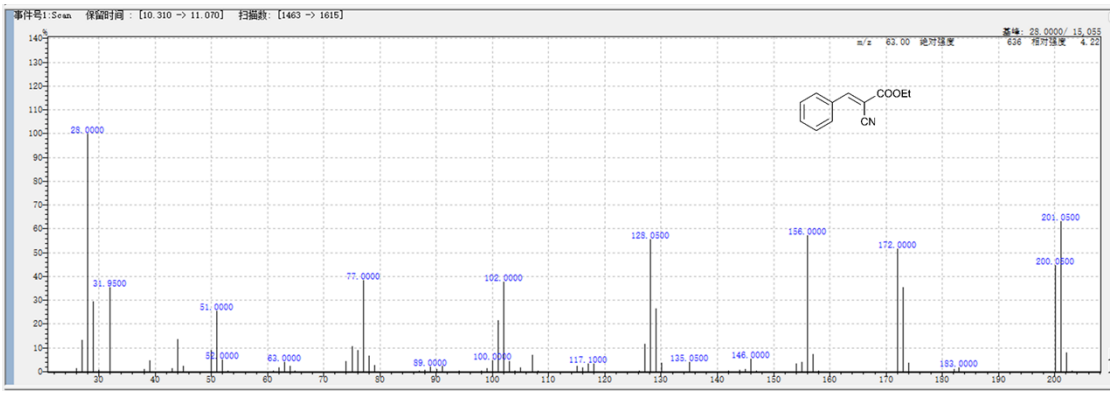

Fig. S22 MS spectrum of compound **3.**

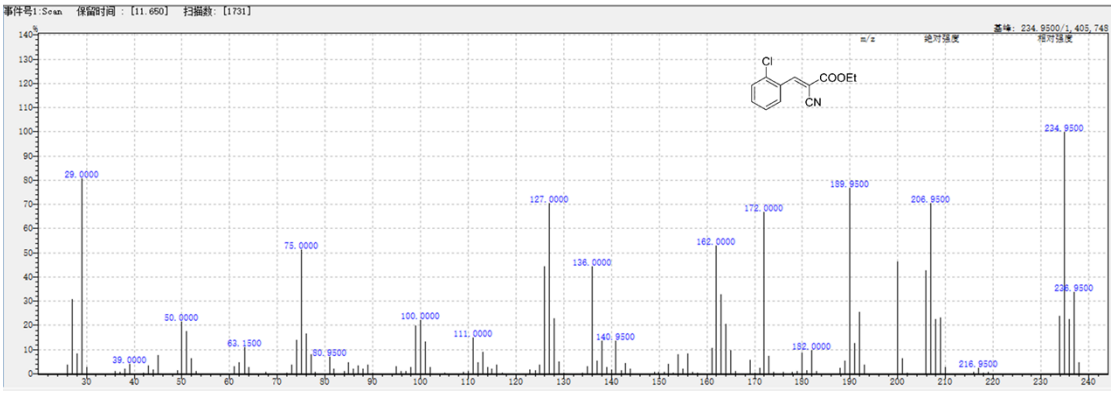

Fig. S23 MS spectrum of compound **3a.**

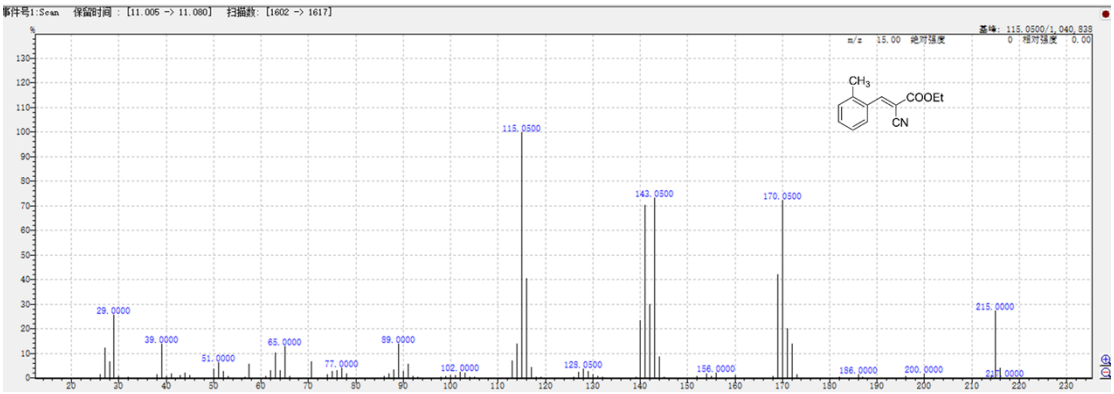

Fig. S24 MS spectrum of compound **3b.**

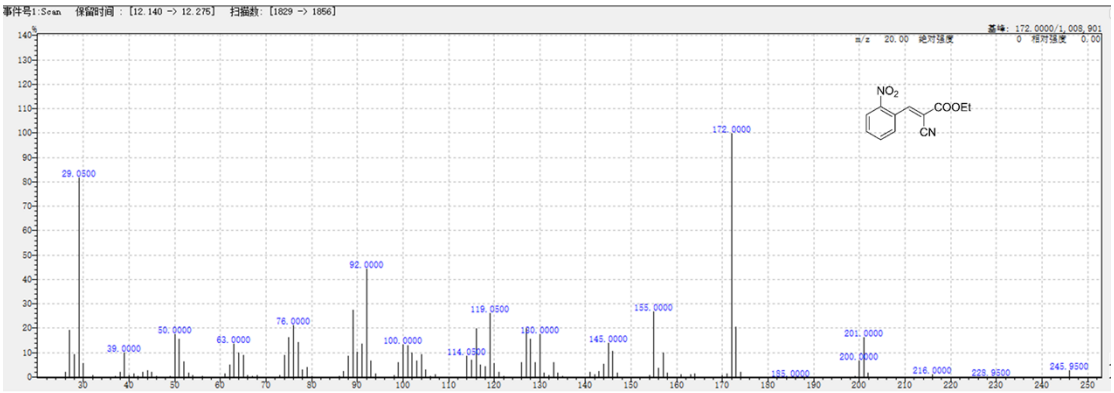

Fig. S25 MS spectrum of compound **3c.**

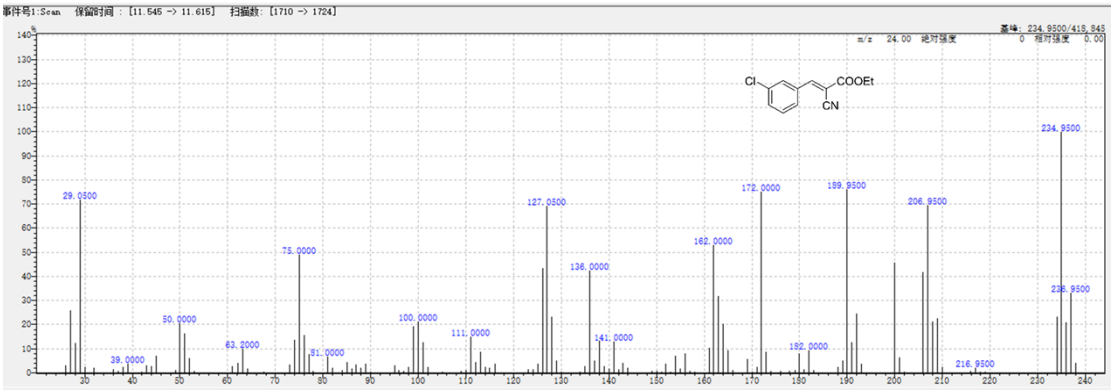

Fig. S26 MS spectrum of compound **3d.**

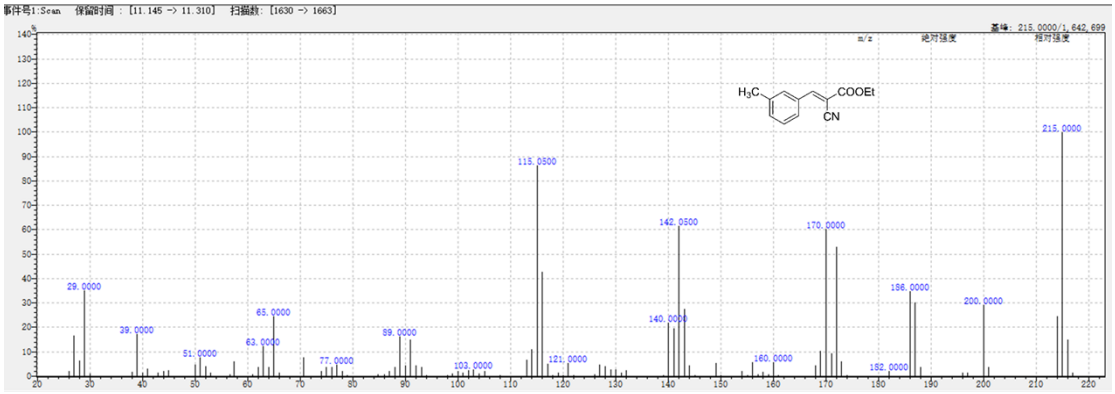

Fig. S27 MS spectrum of compound **3e.**

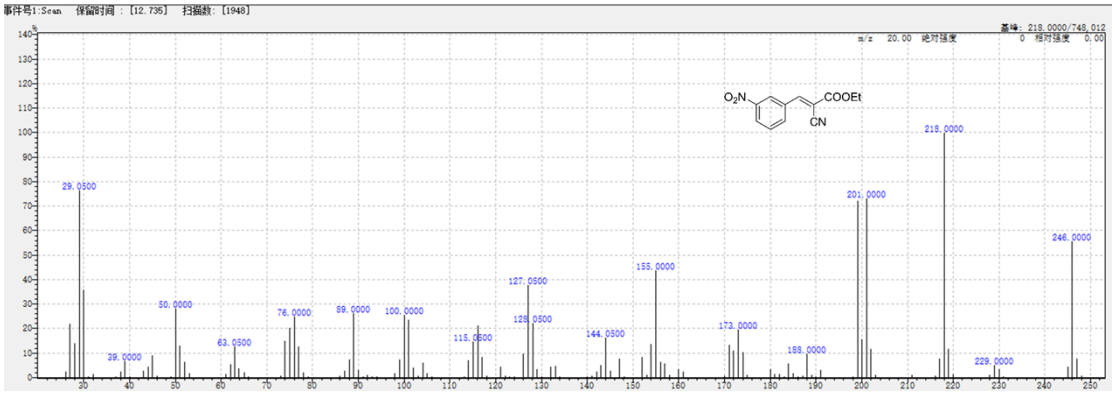

Fig. S28 MS spectrum of compound **3f.**

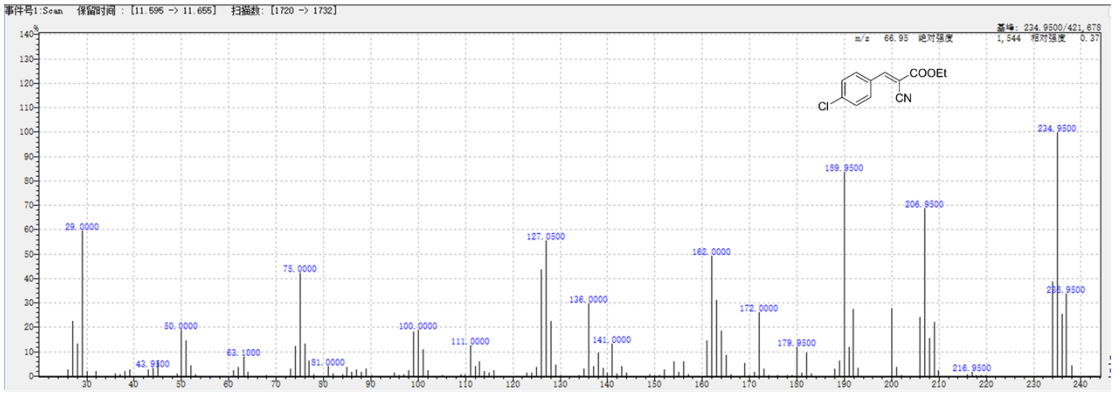

Fig. S29 MS spectrum of compound **3g.**

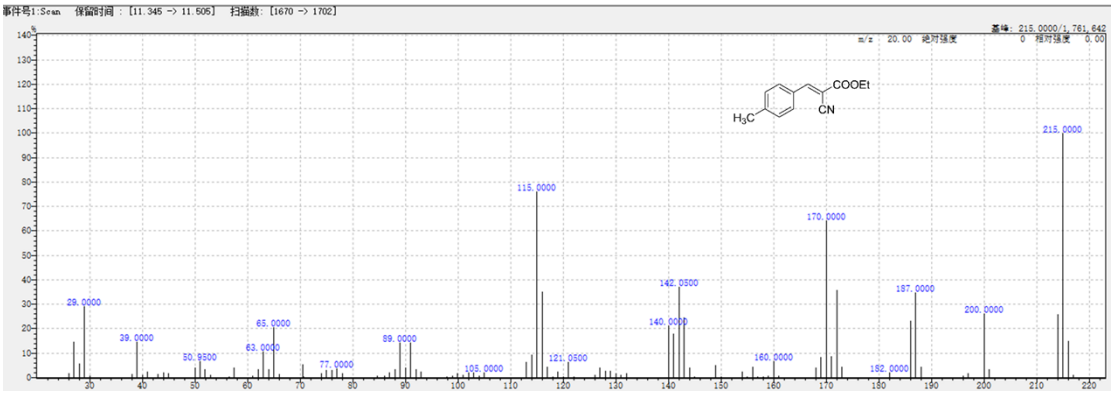

Fig. S30 MS spectrum of compound **3h.**

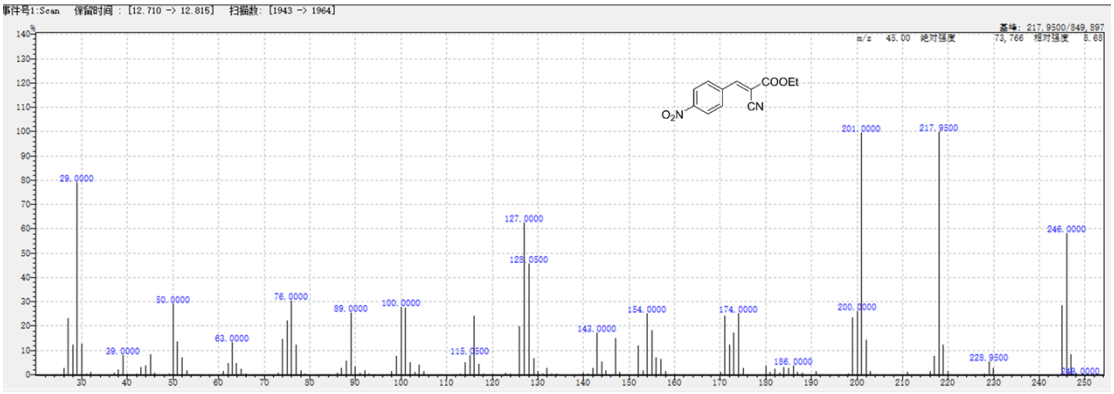

Fig. S31 MS spectrum of compound **3i.**

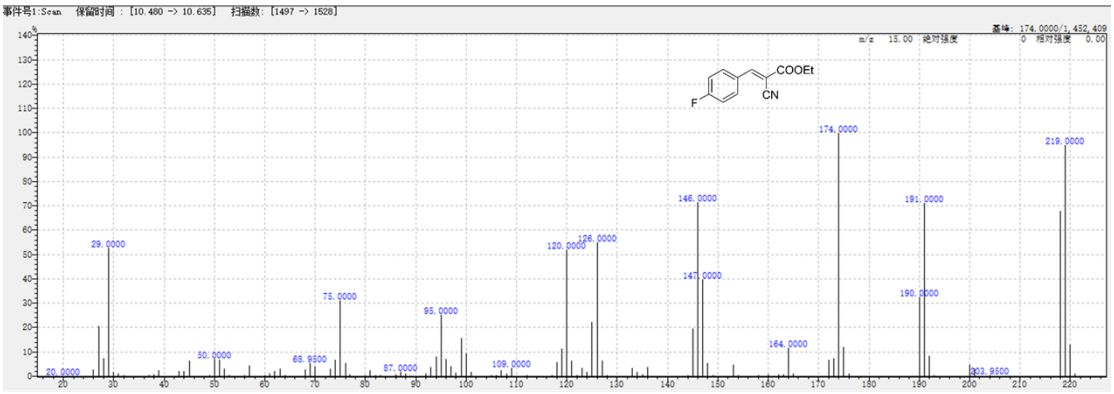

Fig. S32 MS spectrum of compound **3j.**

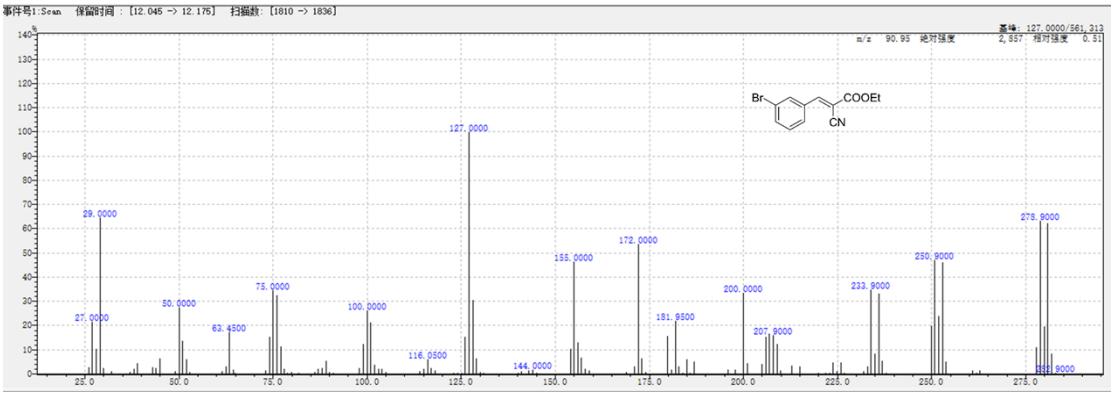

Fig. S33 MS spectrum of compound **3k.**

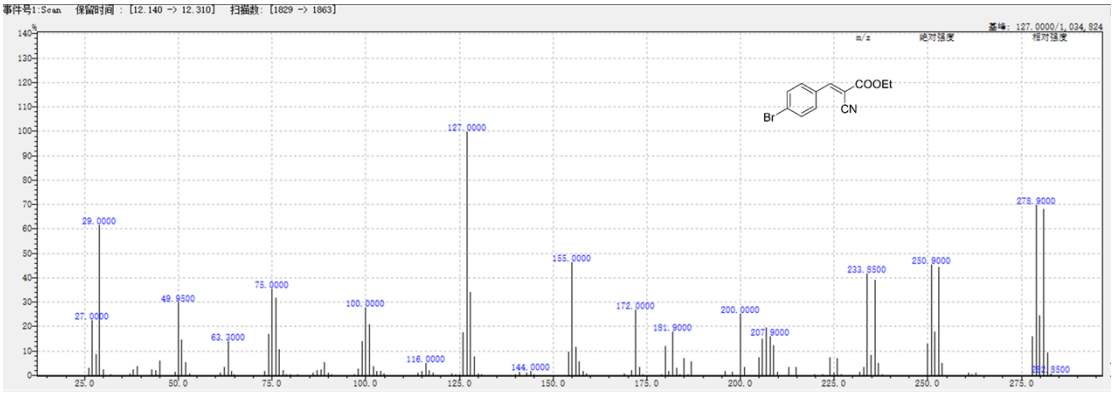

Fig. S34 MS spectrum of compound **3l.**

III. Supplementary Tables

Table S1. Crystal data for compound **Ru_4W_{18}**.

Compound	**Ru_4W_{18}**
Empirical formula	$H_{50}K_8Na_3O_{100}Ru_4W_{18}$
Formula weight	5745.75
temperature (K)	150.02
Crystal system	triclinic
Space group	*P*-1
a [Å]	11.9922(3)
b [Å]	12.0664(3)
c [Å]	15.9420(4)
α /°	84.1350(10)
β /°	81.9160(10)
γ /°	73.4810(10)
Volume/Å^3	2184.95(10)
Z	1
ρ_{calc} g/cm^3	4.367
μ/mm^{-1}	24.778
Crystal size/mm^3	0.2 × 0.1 × 0.08
2*θ* range/deg	4.51 to 50.198
index ranges	-12 ≤ h ≤ 14

	-14 ≤ k ≤ 14
	-19 ≤ l ≤ 19
Reflections collected	27258
Independent reflections	7766
data/restraints/parameters	7766/49/649
GOF on F^2	1.075
R_1, wR_2 [$I \geq 2\sigma(I)$]	0.0274, 0.0663
R_1, wR_2 [all data]	0.0295, 0.0675

[a] $R_1=\Sigma||F_o|-|F_c||/\Sigma|F_o|$. [b] $wR_2=\{\Sigma[w(F_o^2-F_c^2)^2]/\Sigma[w(F_o^2)^2]\}^{1/2}$

Table S2. BVS values of Ru and W atoms of **Ru_4W_{18}**.

Atom	BVS	Atom	BVS	Atom	BVS	Atom	BVS
Ru1	3.015	Ru2	3.231	W1	5.964	W2	6.113
W3	6.306	W4	6.065	W5	6.096	W6	6.023
W7	6.021	W8	6.004	W9	6.042		

Table S3. Selected bond distances of compound **Ru_4W_{18}**.

Bond	Length	Bond	Length	Bond	Length
Ru1–O1	2.052(6)	Ru1–O2	1.988(6)	Ru1–O4	1.980(6)
$Ru1^8$–O10	2.010(6)	Ru1–O17	2.090(6)	Ru1–O22	2.032(6)
$Ru2^8$–O1	2.045(6)	Ru2–O2	2.008(6)	Ru2–O3	2.011(6)
$Ru2^8$–O4	2.037(6)	Ru2–O7	2.008(6)	Ru2–O4	1.961(6)
W1–O1	1.942(6)	W1–O5	1.990(6)	W1–O6	2.195(6)
W1–O11	1.864(6)	W1–O16	1.944(6)	W1–O35	1.725(6)
W2–O3	1.814(6)	W2–O14	2.249(6)	W2–O9	1.958(6)
W2–O12	1.907(6)	W2–O23	1.996(7)	W2–O31	1.735(6)
W3–O2	1.999(6)	W3–O5	1.879(7)	W3–O9	1.927(6)
W3–O13	1.885(6)	W3–O14	2.258(6)	W3–O30	1.735(6)
W4–O13	2.000(6)	W4–O14	2.287(6)	W4–O19	1.915(6)

W4–O23	1.912(6)	W4–O24	1.844(6)	W4–O34	1.723(6)
W5–O10	1.818(6)	W5–O12	1.918(6)	W5–O15	1.977(6)
W5–O20	2.280(6)	W5–O27	1.977(6)	W5–O29	1.720(6)
W6–O6	2.150(6)	W6–O7	1.797(6)	W6–O8	2.019(6)
W7–O6	2.172(6)	W7–O8	1.898(6)	W7–O16	1.954(6)
W8–O15	1.910(6)	W8–O18	2.050(6)	W8–O20	2.241(6)
W9–O24	1.993(6)	W9–O27	1.916(6)	W9–O33	1.721(6)

Table S4. Selected bond angles (°) of compound $\mathbf{Ru_4W_{18}}$.

Bond	Angle	Bond	Angle	Bond	Angle
O1–Ru1–O17	97.4(3)	O1–Ru1–Ru2	40.58(18)	O10–Ru1–O1	89.4(3)
O10–Ru1–O17	82.5(3)	O10–Ru1–O22	88.0(3)	O10–Ru1–Ru2	137.4(2)
O17–Ru1–Ru2	140.03(19)	O2–Ru1–O10	172.1(3)	O2–Ru1–O17	89.6(3)
O1–Ru1–O2	92.2(3)	O2–Ru1–O22	90.5(3)	O2–Ru1–Ru2	50.41(18)
O22–Ru1–O1	177.2(3)	O22–Ru1–O17	83.3(3)	O22–Ru1–Ru2	138.34(18)
O4–Ru1–7O1	80.7(3)	O4–Ru1–O2	99.4(3)	O4–Ru1–O10	88.5(3)
O4–Ru1–O17	170.8(3)	O4–Ru1–O22	98.1(3)	O4–Ru1–Ru2	49.07(18)
O1–Ru2–Ru1	133.50(18)	O1–Ru2–Ru2	40.78(18)	O2–Ru2–O1	176.2(3)
O2–Ru2–O3	88.9(3)	O2–Ru2–O4	98.2(3)	O2–Ru2–Ru1	49.62(19)
O2–Ru2–Ru2	102.07(19)	O3–Ru2–O1	87.9(3)	O3–Ru2–O4	88.1(3)
O3–Ru2–Ru1	138.54(19)	O3–Ru2–Ru2	130.3(2)	O4–Ru2–O1	83.8(3)
O1–W1–O5	86.4(3)	O1–W1–O6	87.5(2)	O11–W1–O1	91.6(3)
O5–W1–O6	88.8(2)	O5–W1–W7	87.84(19)	O6–W1–W7	42.04(17)
O23–W2–O14	71.9(2)	O3–W2–O9	90.3(3)	O4–W2–O12	94.9(3)
O5–W2–O14	88.2(3)	O6–W2–O23	160.0(3)	O12–W2–O3	100.9(3)
O13–W3–142	75.3(3)	O7–W3–O2	100.1(3)	O8–W3–O5	102.4(3)
O9–W3–O9	101.7(3)	O10–W3–O13	99.6(3)	O11–W3–O14	173.4(3)
O29–W5–O27	98.5(3)	O11–W6–O6	74.6(2)	O25–W6–O6	92.6(3)
O26–W6–O8	93.6(3)	O21–W7–O16	163.5(3)	O21–W7–O19	85.7(3)

O28–W7–O8	96.5(3)	O28–W7–O16	97.0(3)	O28–W7–O19	98.4(3)
O22–W8–O15	93.2(3)	O22–W8–O18	157.9(3)	O22–W8–O20	85.5(3)

Table S5. Comparison of the catalytic efficiency of different heterogeneous catalysts.

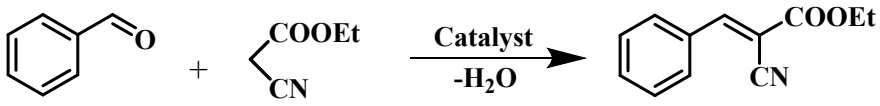

Entry	Catalysts	Amount	Temp(°C)	Time(h)	solvent	Yield	Ref.
1	**Ru_4W_{18}**	0.1 mol%	70	3	ethanol	95.8	This work
2	Na-A-PW_9	2.25 mol%	rt	6	methanol	80	[9]
3	Na-B-PW_9	2.25 mol%	rt	6	methanol	83	[9]
4	$Na_{16}[SiNb_{12}O_{40}]\cdot xH_2O$	0.05 g	70	2	methanol	97.2	[10]
5	PIC 3_Nb	0.01 mol	80	6	ethanol	83	[11]
6	Mg_3Al-PW_{12}	3.0 mol%	60	6	2-propanol and water	99	[12]
7	Tris-LDH-$Zn_4(PW_9)_2$	0.01mmol	80	6	CH_3CN	99	[13]
8	$K_7HNb_6O_{19}\cdot 13H_2O$	5 μmol	60	2	ethanol	98	[14]
9	$(NH_4)_{17}Na_7H_{12}[Co(H_2O)TeMo_6O_{21}\{N(CH_2PO_3)_3\}]_6\cdot 42H_2O$	0.03 mol%	70	3	methanol	92	[15]
10	$(NH_4)_6Na_3H_{13}[TeMo_{10}O_{37}(CoMo_2O_6L)_4]\cdot 11H_2O$	0.15 mol %	70	3	ethanol	92	[16]

References

1. C. M. Tourné and G. F. Tourné, *J. Chem. Soc., Dalton Trans.*, 1988, DOI: 10.1039/dt9880002411, 2411-2420.
2. G. M. Sheldrick, *Acta Crystallogr., Sect. A:Found. Crystallogr*, 2007, **64**, 112-122.
3. G. M. Sheldrick, *Acta Crystallogr., Sect. A:Found. Crystallogr*, 2015, **71**, 3-8.
4. A. R. Howells, A. Sankarraj and C. Shannon, *J. Am. Chem. Soc*, 2004, **126**, 12258-12259.
5. Y. V. Geletii, B. Botar, P. Kögerler, D. A. Hillesheim, D. G. Musaev and C. L. Hill, *Angew. Chem., Int. Ed*, 2008, **47**, 3896-3899.

6. A. Sartorel, M. Carraro, G. Scorrano, R. D. Zorzi, S. Geremia, N. D. McDaniel, S. Bernhard and M. Bonchio, *J. Am. Chem. Soc*, 2008, **130**, 5006-5007.
7. C. Besson, Z. Huang, Y. V. Geletii, S. Lense, K. I. Hardcastle, D. G. Musaev, T. Lian, A. Proust and C. L. Hill, *Chem. Commun*, 2010, **46**.
8. S. Yamaguchi, K. Uehara, K. Kamata, K. Yamaguchi and N. Mizuno, *Chem. Lett*, 2008, **37**, 328-329.
9. S. Zhao, Y. Chen and Y.-F. Song, *Appl. Catal., A*, 2014, **475**, 140-146.
10. W. Ge, X. Wang, L. Zhang, L. Du, Y. Zhou and J. Wang, *Catal. Sci. Technol*, 2016, **6**, 460-467.
11. Z. Weng, N. Ogiwara, T. Kitao, Y. Kikukawa, Y. Gao, L. Yan and S. Uchida, *Nanoscale*, 2021, **13**, 18451-18457.
12. Y. Jia, Y. Fang, Y. Zhang, H. N. Miras and Y. F. Song, *Chem. - Eur. J*, 2015, **21**, 14862-14870.
13. K. Liu, Y. Xu, Z. Yao, H. N. Miras and Y. F. Song, *ChemCatChem*, 2016, **8**, 929-937.
14. Q. Xu, Y. Niu, G. Wang, Y. Li, Y. Zhao, V. Singh, J. Niu and J. Wang, *Mol. Catal*, 2018, **453**, 93-99.
15. Q. Xu, B. Xu, H. Kong, P. He, J. Wang, T. Kannan, P. Ma, J. Wang and J. Niu, *Inorg. Chem*, 2020, **59**, 10665-10672.
16. H. Kong, B. Xu, J. Zhen, S. Liu, K. Li, P. Ma, J. Wang and J. Niu, *Inorg. Chem*, 2021, **60**, 14872-14879.